ACS APPLIED MATERIALS & INTERFACES

Forum Article

www.acsami.org

Optical Properties and Exciton Dynamics of Alloyed Core/Shell/Shell $Cd_{1-x}Zn_xSe/ZnSe/ZnS$ Quantum Dots

Bob C. Fitzmorris,[†,‡] Ying-Chih Pu,[†,§] Jason K. Cooper,[‡] Yi-Fang Lin,[§] Yung-Jung Hsu,[*,§] Yat Li,[‡] and Jin Z. Zhang[*,‡]

[‡]Department of Chemistry and Biochemistry, University of California, Santa Cruz, California 95064, United States

[§]Department of Materials Science and Engineering, National Chiao Tung University, 1001 University Road, Hsinchu 30010, Taiwan, Republic of China

ABSTRACT: In this study we introduce a new method for the one-pot synthesis of core/shell/shell alloyed $Cd_{1-x}Zn_xSe/ZnSe/ZnS$ QDs and examine the effect of the shell coating on the optical properties and exciton dynamics of the alloy core. The photoluminescence (PL) quantum yield is greatly enhanced after shell growth, from 9.6% to 63%. The exciton dynamics were studied by time correlated single photon counting (TCSPC) and fit using integrated singular value decomposition global fitting (i-SVD-GF), which showed the biexponential observed lifetimes on the nanosecond time scale remain the same after shell growth. Using ultrafast transient absorption (TA) spectroscopy and SVD-GF, we have determined that surface passivation by ZnSe and ZnSe/ZnS shells reduces nonradiative recombination primarily on the picosecond time scale. These findings are helpful in directing the development of the next generation of QDs for biological labeling and other applications.

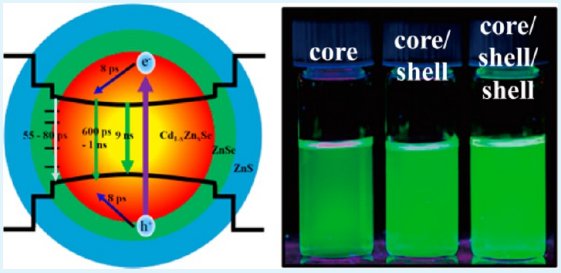

KEYWORDS: *quantum dot, alloy, core/shell, core/shell/shell, shell, time-resolved, fluorescence, photoluminescence, quantum yield, biological labeling, exciton, dynamics, transient absorption, ultrafast, CdSe, ZnSe, ZnS*

1. INTRODUCTION

Quantum dots (QDs) have generated great fundamental and technological interest because of their novel size-tunable optical properties[1,2] and, consequently, potential applications in light emitting diodes,[3,4] photovoltaics[5−7] and biomedical tags.[8−10] In QDs, the three-dimensional confinement of the exciton and the size-dependent energy levels result in the possibility of tuning the bandgap to a desired energy by controlling the particle size.[11,12] Due to this quantum size confinement effect, it is possible to tune the QD absorption and emission spectra throughout a wide wavelength range.[13] For example, when the particle size of CdSe is increased from 2 to 4 nm, the bandgap would reduce from 2.6 to 2.1 eV, and the corresponding emission wavelength would red shift from 530 to 630 nm.[13] One important issue for QDs is that the surface-to-volume (S/V) ratio increases with decreasing size proportional to 3/r, which renders them highly sensitive to their environment and consequently more susceptible to quenching of the photoluminescence (PL) through surface trap states. Surface trapping has been a major obstacle limiting the PL quantum yield (QY) and thereby applications of small and highly confined blue and green emitting QDs such as CdSe.

Recently, ternary alloyed QDs have received great attention because of their composition-tunable bandgap and PL emission across the visible spectrum without changing particle size.[14,15] The PL QYs of alloyed $Cd_{1-x}Zn_xSe$ QDs are often higher than those of single component QDs; in particular, the green emitting alloyed $Cd_{1-x}Zn_xSe$ QDs have higher PL QY than green emitting CdSe.[14] Moreover, the alloyed QDs have shown interesting properties that are not observed in the binary QD systems such as the core/shell $Cd_{1-x}Zn_xSe/ZnSe$ QDs that showed unusual nonblinking behavior in absolute contrast to CdSe-based QDs whose PL turns on and off intermittently.[16] Nonblinking alloyed QDs would be very useful in applications that require a continuous output of photons such as light-emitting diodes, photoelectrodes or biolabeling.[17]

For applications of QDs requiring high PL QY, it is important to passivate surface defects and protect the QDs from the surrounding environment.[18,19] Generally, the surface is passivated using organic ligands or an inorganic shell material. Organic ligands serve several purposes including stabilizing monomers during QD growth, directing the size and shape of QDs, as well as bonding to surface trap states on the QD creating new electronic states outside of the band gap.[20,21] Although individual organic ligands can efficiently passivate surface trap states, the steric hindrance between adjacent ligands makes complete surface coverage unrealistic.[22]

Inorganic shell materials can achieve more complete surface coverage than organic ligands but they suffer from a trade-off

Special Issue: Forum on Biomedical Applications of Colloidal Photoluminescent Quantum Dots

Received: December 17, 2012
Accepted: March 7, 2013
Published: March 7, 2013

   dx.doi.org/10.1021/am303149r | *ACS Appl. Mater. Interfaces* 2013, 5, 2893−2900

that makes choosing a single shell material difficult. For CdSe, the most popular type I shell materials, shell materials that have a wider bandgap than the core, include ZnSe, CdS, and ZnS. ZnSe and CdS share a common atom with the core material and have crystal lattice spacings and band energies similar to those of CdSe.[23,24] ZnS has a larger lattice mismatch with CdSe than the others and its valence and conduction band energies straddle those of CdSe insulating the core excitons from reaching the QD surface.[21,25] Compared to ZnS, ZnSe and CdS can be grown more easily onto CdSe with more complete surface coverage due to the small lattice mismatch between the materials. However, ZnS has a wider bandgap which can more efficiently confine excitons to the CdSe core than ZnSe or CdS.

Recently, several studies have shown that core/shell/shell QDs composed of either CdSe/ZnSe/ZnS or CdSe/CdS/ZnS have the advantages of a small lattice mismatch at the core/shell interface and a large difference in band edge positions between core and shell materials.[19,26−29] In our previous study, we demonstrated a one-pot synthesis for core/shell/shell (CSS) CdSe/ZnSe/ZnS QDs that greatly increases the quantum yield of the CdSe core and improves stability of the PL.[19] Time-resolved photoluminescence (TRPL) showed that the CSS approach improves the PL QY of the core CdSe QDs by eliminating a fast nonradiative recombination pathway associated with surface dangling bonds in CdSe or lattice dislocations in core/shell CdSe/ZnS.

In this study, we investigate the ability of type I shells to passivate the surface of alloyed QDs, a necessary step in their application in biological labeling. We developed a facile one-pot synthesis approach to fabricate alloyed core/shell/shell (aCSS) $Cd_{1-x}Zn_xSe$/ZnSe/ZnS QDs with high QY. TRPL measurements were conducted to explore the exciton dynamics in alloy core (aC) $Cd_{1-x}Zn_xSe$ QDs, alloyed core/shell (aCS) $Cd_{1-x}Zn_xSe$/ZnSe QDs and aCSS QDs, respectively. In addition, we have probed exciton dynamics in the QDs using fs transient absorption (TA) spectroscopy to gain insights into nonradiative recombination channels in these systems. The combined results show that the aCSS QDs exhibited efficient surface passivation, high QY, and have great promise in biological and other applications that require highly luminescent QDs.

2. EXPERIMENTAL: MATERIALS AND METHODS

2.1. Chemicals. Cadmium oxide (CdO, 99.99%), zinc acetate (anhydrous 99.9%,powder), zinc stearate (technical grade), selenium (Se 99.9%, powder), sulfur (S 99.9%, powder), trioctylphosphine (TOP, 99%), oleic acid (90%), oleylamine (90%), octadecene (ODE, 90%), dichloromethane (DCM, ACS grade), methanol (99.9%), acetone (99.7%), and hexane (99%). All chemicals were used without further purification.

2.2. One-Pot Synthesis of Alloyed $Cd_xZn_{1-x}Se$/ZnSe/ZnS aCSS QDs. QDs were synthesized by combining two previously reported methods. Alloyed core QDs were synthesized using a hot-injection method modified from Lee et al[30] while the shell growth was adapted from our previously reported synthesis of core/shell/shell CdSe/ZnSe/ZnS QDs using successive injection of precursors in one pot.[18,19] Typically, 0.12 mmol of cadmium oxide, 0.88 mmol of zinc acetate (anhydrous), 5 mL of oleic acid, 5 mL of oleylamine and 5 mL of ODE were placed in a 50 mL of round-bottom flask. The mixture was heated to 120 °C, degassed under vacuum for 30 min, filled with Ar gas and further heated to 230 °C. After the mixture formed a clear solution, the reaction temperature was dropped to 120 °C, the solution was degassed under vacuum for another 30 min, filled with Ar gas and heated to 320 °C. Meanwhile, a solution containing 1.5 mmol of Se powder and 1.5 mL of TOP was prepared in a N_2 filled glovebox. The TOP:Se solution was removed from the glovebox in a septum top vial, heated to 280 °C and quickly injected into the reaction flask without exposing the solution to air.[31] After the injection, the temperature of the reaction flask was kept at 320 °C for 60 min to grow aC QDs, after which an aliquot (~1 mL) was taken from the reaction and the solution was cooled down to 240 °C for further shell coating. The ZnSe shell was formed by injecting a suspension of TOP:Se solution (0.078 g of Se and 1 mL of TOP) dropwise over a period of 5 min, then adding 0.1 g of zinc stearate in 0.77 g of ODE in the same way. After allowing the solution to react for about ten minutes, an aliquot of the aCS QDs was taken. To grow the ZnS shell, the reaction mixture was cooled to 200 °C, and a suspension of 0.1 g of zinc stearate in 0.77 g ODE was added dropwise first and subsequently, a suspension of 0.035 g S in 0.61 mL TOP was added dropwise over 5 min. The resulting solution was allowed to react for 20 min at 200 °C and then cooled to room temperature. The QD samples were washed and collected by the following procedure. The reaction mixture was diluted with hexanes, ethanol was added, and the mixture was shaken vigorously and centrifuged to remove excess ligands and precursors. After repeating the process three times, the precipitated QD samples were redispensed in hexane for further UV−vis, PL, TEM, TA, and TRPL measurements.

2.3. UV−Visible and Photoluminescence Spectroscopy. The UV−visible absorption (UV−vis) spectra were recorded at room temperature using Hewlett-Packard 8452A diode array spectrometer with spectral resolution set to 2 nm. A Perkin-Elmer model LS50B luminescence spectrometer was used to obtain the PL spectra at room temperature. Calculation of the PL quantum yield of QDs was accomplished by comparing the integrated PL intensity of the QDs (PL_{QD}) in hexane to that of perylene dye (PL QY_{dye} = 0.95)[32] in ethanol taking into account the absorption of each QD sample (Abs_{QD}) and the dye (Abs_{dye}) at the excitation wavelength (388 nm), the temperature, and the refractive index (n) of the solvents.

$$QY = QY_{dye}\frac{PL_{QD}}{PL_{dye}}\frac{Abs_{dye}}{Abs_{QD}}\frac{n_{hexane}}{n_{ethanol}} \quad (1)$$

2.4. Transient Absorption Spectroscopy. The TA laser system used in this study has been described previously.[33] In this study, a pump wavelength of 480 nm, generated by an OPA, with a repetition rate of 752 Hz was chosen to excite only the core material in the sample. The sample was probed with a white light continuum which is stable from 430 to 800 nm with a pulse width of 100 fs. Temporal resolution of 50 fs is achieved through a motor-controlled delay state. 4000 signal averages were taken for each time point. Both forward and reverse delay scans were collected and averaged. Optically clear dispersions were prepared in hexanes. Data was analyzed using Matlab and singular value decomposition (SVD) in which 3 basis vectors were kept from the U and V matrices. The resulting time dependence in the V matrix was fit with a triple exponential shown in eq 2. These global fitting procedures developed in house and reported previously.[18,19,34]

2.5. Time-Resolved Photoluminescence. Observed PL lifetimes were measured using a time correlated single photon counting (TCSPC) system described previously. Briefly, a 5 W Coherent Verdi-V5 (532 nm) continuous wave laser was used to pump a tunable (790−820 nm), mode locked Ti:sapphire laser (Kapteyn-Murnane Laboratories, model: MTS Mini) operating at a repetition rate of 200 MHz. A wavelength of 800 nm was passed through a pulse picker (Conoptics, model 350−160) to increase the time between pulses to 50 ns. This near 800 nm light was then frequency doubled to 400 nm using a bismuth borate (BBO) crystal which was used to excite the QD sample dispersed in hexanes. The QD PL was collected at a 90° angle and passed through a magic angle polarizer and into a monochromator. The monochromatic photons were counted using an avalanche photodiode operated in reverse start stop mode. The instrument response function was 50 ps. The decay spectrum was recorded at 10 nm steps from 490 to 590 nm which encompassed the majority of the PL peak from the aC, aCS, and aCSS samples. Each decay trace was normalized to collection time and was used to reconstruct the PL decay spectrum which was subsequently

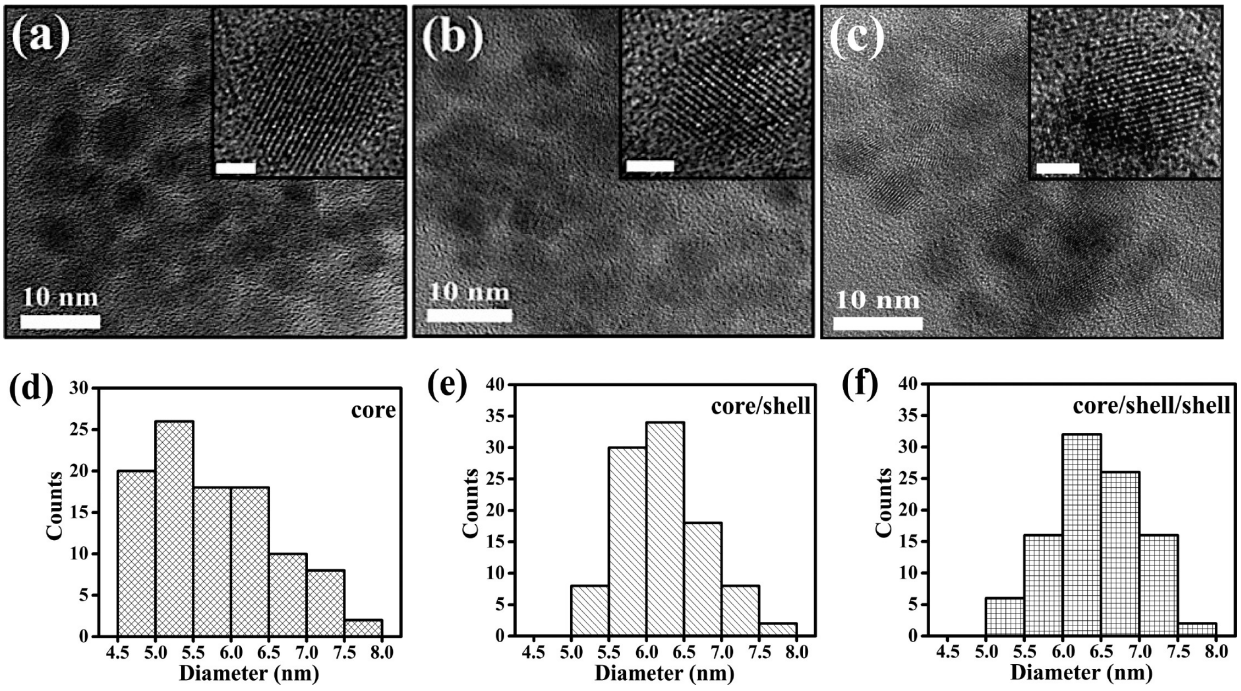

Figure 1. TEM images of the (a) aC QDs, (b) aCS QDs, and (c) aCSS QDs. The insets are HR-TEM images with 2 nm scale bars. Histograms showing the distribution of the diameter for (d) aC QDs, (e) aCS QDs, and (f) aCSS QDs.

deconvoluted with SVD and fit globally using a double exponential function shown in eq 2. The resulting B-spectrum indicating individual spectral decay components were integrated using eq 3 to report the photon flux.

2.6. Transmission Electron Microscopy. Transmission electron microscopy (TEM) images of aC, aCS and aCSS QDs were recorded by high-resolution transmission electron microscopy (HRTEM, JEOL JEM-3000) operated at 300 kV. The samples were supported by a copper grid with carbon film.

3. RESULTS

3.1. Structural Determination Using TEM. Figure 1 shows TEM images of aC, aCS, and aCSS QDs. All of the samples are near spherical in shape with a narrow size distribution. The average diameter of aC, aCS and aCSS QDs determined from measuring 100 QDs of each type were 5.9 ± 0.8, 6.3 ± 0.3, and 6.4 ± 0.4 nm, respectively. The well-resolved lattice fringes of QD samples can be clear seen in the insets of Figure 1.

3.2. Optical Properties. UV−vis absorption and PL emission spectra for aC, aCS and aCSS QDs are presented in Figure 2. The UV−vis absorption spectra show that the first excitonic peak positions are identical for aC and aCS QDs at 536 nm while that of the aCSS sample is at 534 nm. The solutions of QDs were diluted in hexanes prior to PL measurements to obtain the same absorption for all samples at 388 nm, the excitation wavelength used for PL measurements. The PL spectra show that the emission maximum blue-shifts as shells are grown from 549 nm for the aC to 548 nm for aCS and to 543 nm for aCSS. The PL quantum yield (QY) samples also increases from 9.6% for aC to 42% for aCS and to 63% for aCSS. The progressively stronger PL of aCSS QD samples can be seen under normal indoor light or in the dark with UV irradiation as shown in Figure 3.

3.3. Exciton Dynamics via Transient Absorption Spectroscopy. Ultrafast transient absorption (TA) spectroscopy was used to investigate exciton dynamics on the picosecond (ps) time scale. TA spectra were taken using a pump wavelength of 480 nm that was attenuated using neutral density filters in order to record TA data at several pump powers for each sample. A representative contour plot of the TA data for the aCSS QD sample is shown in Figure 4a of the differential absorption (dA) as a function of both probe

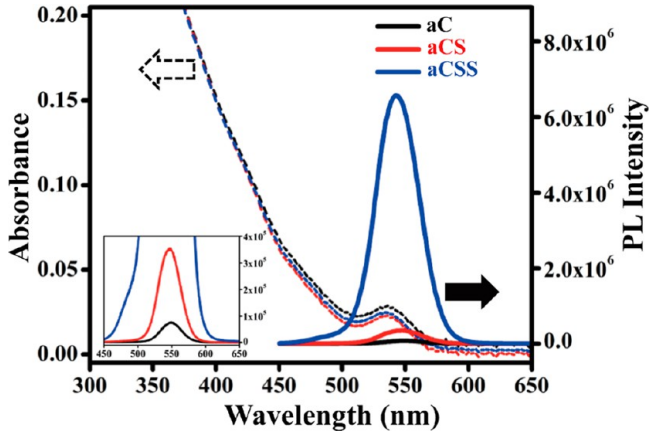

Figure 2. UV−vis and PL spectra for aC QDs, aCS QDs, and aCSS QDs.

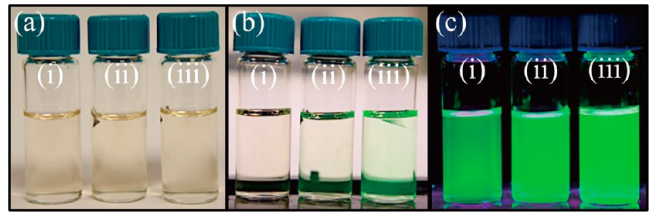

Figure 3. Photograph of the solutions of (i) aC QDs, (ii) aCS QDs, and (iii) aCSS QDs (a) under normal indoor light, (b) under normal indoor light with UV light, and (c) in the dark with UV light.

dx.doi.org/10.1021/am303149r | ACS Appl. Mater. Interfaces 2013, 5, 2893−2900

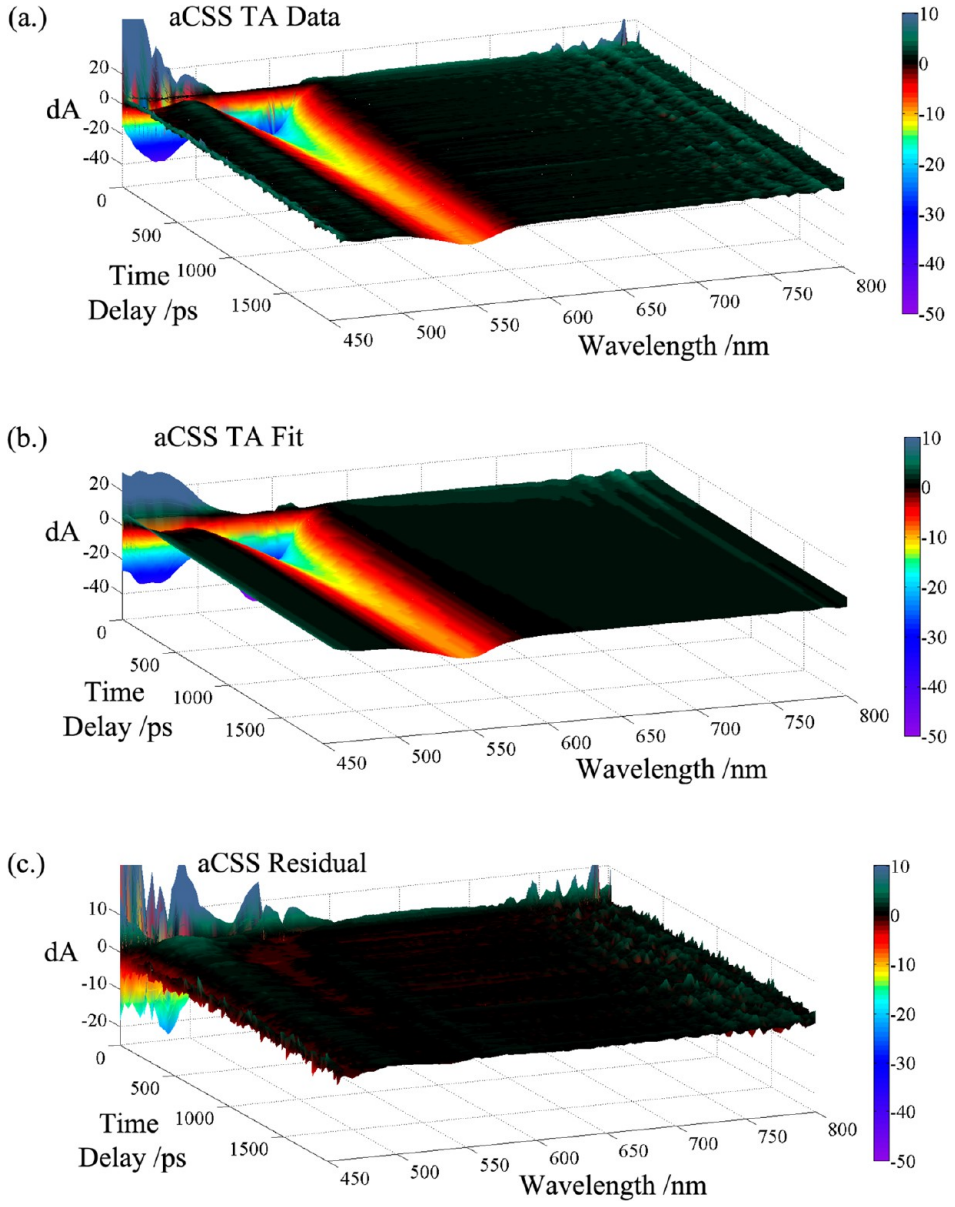

Figure 4. Contour plots of the TA data for aCSS QDs excited with 480 nm light. (a) The raw data dA vs time delay and probe wavelength. (b) Triple exponential fit of the data. (c) Plot of the residual data that were not fit (data − fit) showing no wavelength or time dependence.

Table 1. Summary of PL QY and Exciton Lifetimes Found from Global Fitting of TA Data

sample	PL QY (%)	TA τ_1 (ps)	TA τ_2 (ps)	TA τ_3 (ps)	TRPL τ_1 (ns)	τ_1 % of PL	TRPL τ_2 (ns)	τ_2 % of PL
aC QDs	9.6	7 ± 1	55 ± 7	600 ± 50	1.1 ± 0.2	8	9 ± 1	92
aCS QDs	42	8 ± 1	80 ± 10	700 ± 80	1.2 ± 0.2	5	10 ± 1	95
aCSS QDs	63	8 ± 1	80 ± 10	700 ± 80	1.1 ± 0.2	7	9 ± 1	93

wavelength and time delay following the pump pulse. The dominant features are two transient bleach (negative dA) recovery features centered at 540 and 480 nm. The 540 nm feature is much slower and does not completely decay within the 2 ns (ns) time window. With higher pump power, the amplitude of the 480 nm bleach feature increases disproportionally relative to the 540 nm bleach. The initial dA spectrum is similar for aC, aCS, and aCSS QDs but the 540 nm bleach feature recovers slowest for aCSS with aCS slightly faster and aC much faster.

A global fitting procedure was employed to find the best exponential lifetimes to fit the decay of the TA signal at every probe wavelength. Equation 2 below was used to describe the triple exponential decay of the TA signal at each wavelength where $I(t)$ is the dA amplitude at time (t), and A_i is the initial intensity of the component of the decay corresponding to the lifetime τ_i.

$$I(t) = \sum_{3}^{i=1} A_i e^{-t/\tau_i} \tag{2}$$

The aCS contour plot was shown in Figure 4a, the resulting fit was shown in Figure 4b, and the residuals were shown in Figure 4c. The residual is the noise in the raw data and exhibits

dx.doi.org/10.1021/am303149r | ACS Appl. Mater. Interfaces 2013, 5, 2893−2900

no wavelength nor time dependence indicating that we have successfully fit all the meaningful data. Lifetimes found from global fitting are 7 ± 1, 55 ± 7, and 600 ± 50 ps for aC and 8 ± 1, 80 ± 10, and 700 ± 80 ps for both aCS and aCSS. These lifetimes are tabulated for the aC, aCS, and aCSS samples in Table 1.

The plot of the initial intensity of each lifetime component, A_i, as a function of probe wavelength is referred to as the b-spectrum. Figure 5 is a plot of the TA b-spectrum for the aC

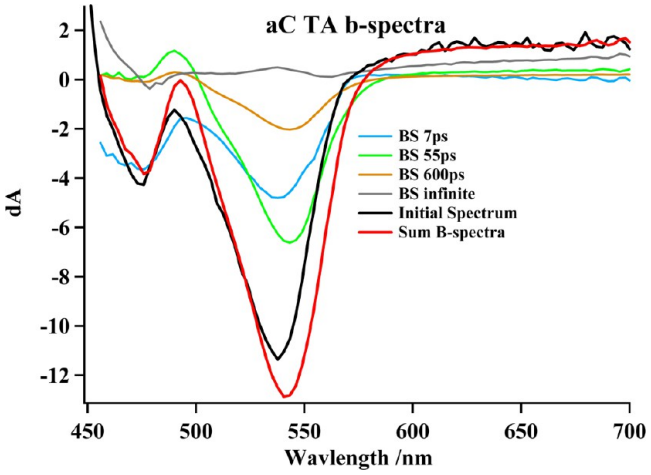

Figure 5. Initial TA spectrum for the aC QDs at the lowest pump power plotted along with the b-spectra of each component of the triple exponential decay. BS 7 ps is the spectral distribution of the fastest component, attributed to the electron−hole plasma generated upon excitation. BS 55 ps is attributed to bound excitons which decay nonradiatively through suface and interface traps. BS 600 is also attributed to exciton recombination, but it could be either radiative or nonradiative recombination. BS infinite is for the *y*-offset; this is the component of the initial TA spectrum that does not decay in the 2 ns time window.

sample along with the initial TA spectrum and the sum of the b-spectra. This plot shows that the recovery of the 480 nm bleach can be described with a 7 ps lifetime single exponential decay while all three lifetimes (7, 55, and 600 ps) contribute to the 540 nm bleach.

Plots of dA vs time for particular probe wavelengths are one of the easiest ways to compare the TA data for different samples. All three samples studied exhibit a spectral feature at 540 nm that is dominant at lower pump power. Figure 6 is a plot of 540 nm decay traces taken at the lowest (top) and highest (bottom) pump power for all three samples. Note that the initial dA for each trace in Figure 6 has been normalized to −1. These single wavelength traces show that at 540 nm, the transient bleach recovery of the aC sample is dominated by the 7 ps component, indicated by its relative amplitude, as compared to the aCS and aCSS samples. The aCS sample has slightly more 7 ps amplitude than the aCSS sample at low power, but this difference becomes particularly apparent at higher pump power.

3.4. Exciton Dynamics via Time-resolved PL Spectroscopy. TRPL decay traces were measured for each of the samples at 10 nm intervals spanning the width of the PL emission peak. The normalized decay traces were very similar for all three samples studied, as shown by the 540 nm TRPL decay traces in Figure 7.

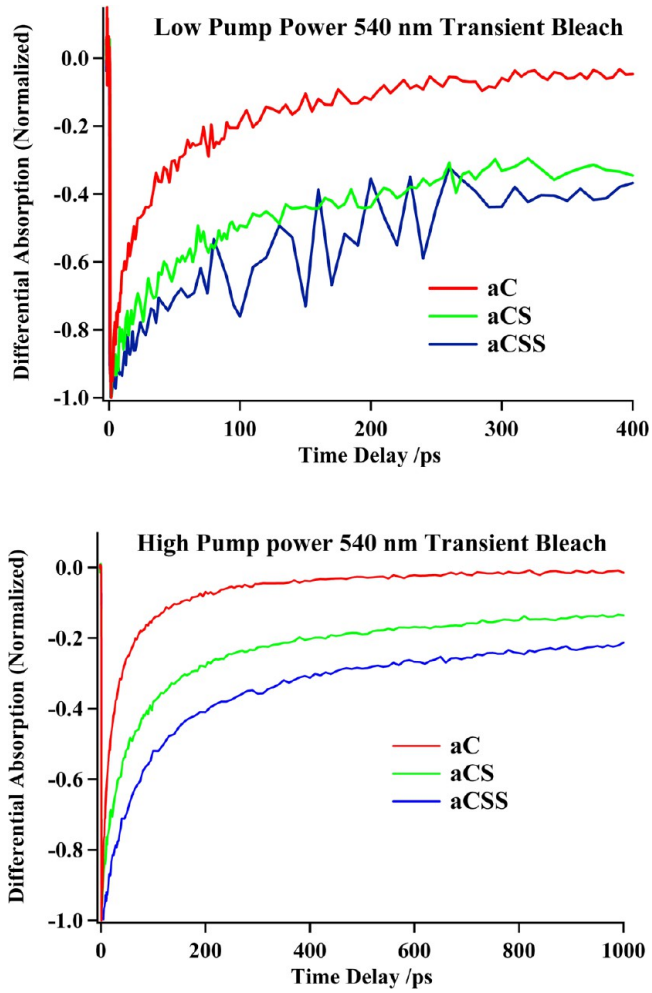

Figure 6. 540 nm bleach recovery traces for aC, aCS and aCSS at the low (top) and high (bottom) pump power. The trend shows that the aC bleach decays the fastest, then aCS then aCSS. This same trend is consistent at higher pump powers and helps describe the high QY of the aCSS sample.

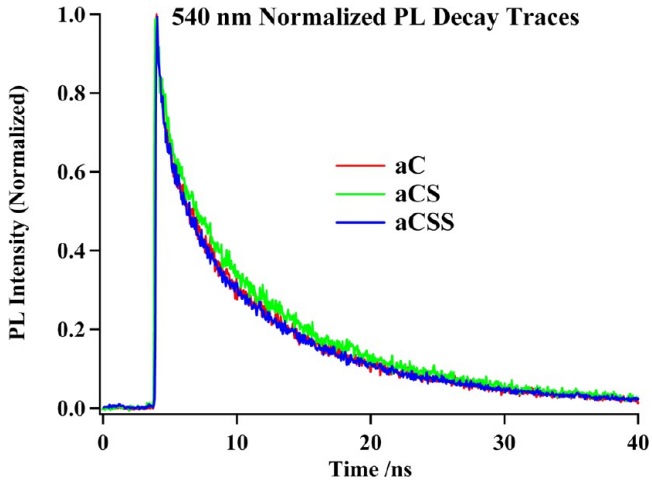

Figure 7. TRPL decay traces taken at an emission wavelength of 540 nm, near the maximum of the PL peak for aC, aCS and aCSS QDs.

SVD-global fitting was used for each sample to the find the best lifetimes that can fit the decay traces at every wavelength. The TRPL of each sample could be fit with a double

exponential function (eq 2) with two lifetimes of about 1.1 ± 0.2 and 9 ± 1.1 ns. Instead of plotting the b-spectra to show how each lifetime contributed to the initial intensity for each decay trace, we have integrated each component of the double exponential decay at each wavelength to determine the overall photon flux, Φ_p, from each component of the decay, eq 3.

$$\Phi_p(\lambda) = \int A_i e^{-t/\tau_i} dt \quad (3)$$

The Φ_p from each of the two lifetimes was plotted for each of the twelve single wavelength decay traces and reported in Figure 8. Each $\Phi_p(\lambda)$ spectral feature was subsequently fit with a Gaussian function in Figure 8. The sum of the two Φ_p Gaussian fits was also reported and compared to the steady-state PL spectrum that was normalized to have the same maximum. There is good agreement between the sum of the Φ_p fits and the steady-state PL spectrum indicating that the steady state PL can be accurately reconstructed using global fitting of the TRPL data. The area under plots of Φ_p are proportional to the contribution of each decay lifetime to the steady state PL spectrum, on average for the three samples the 1.1 ns component contributes 7% of the PL, whereas the 9 ns component contributes 93% of the decay. TRPL lifetimes and their relative contributions to the overall steady state PL are shown in Table 1 for each sample.

4. DISCUSSION

4.1. Structure and PL of the aCSS QDs. The synthesis of the aC QDs resulted in particles that are 5.9 ± 0.8 nm in diameter and emit at 540 nm. Based on the empirical equation developed by Yu et al.,[35] a CdSe QD with a diameter of 5.91 nm would emit at 624 nm, whereas a CdSe QD would have to be about 2.9 nm in diameter to emit at 540 nm. It is clear from the size and emission wavelength that the aC QDs are not purely CdSe and they cannot be pure ZnSe, which has a bulk band gap of 2.69 eV that corresponds to 460 nm emission. Besides alloying, another possible explanation for the emission and size discrepancy would be a core shell structure composed of a small CdSe core (less than 3 nm) and a thick ZnSe shell. This is unlikely because injection of additional ZnSe precursors after the growth of aC QDs resulted in a dramatic increase in the PL QY (9.6% → 42%) with no significant change to the emission spectrum. If a ZnSe shell was already present prior to the intentional ZnSe shell growth, then the additional shell would not have such a dramatic effect on the PL QY. PL QY was improved further, to 62%, after the addition of ZnS precursors and again the emission wavelength did not shift significantly from aC to aCS and finally to aCSS. Additional evidence for the presence of an insulating shell on the aCSS QDs is that they were able to retain their PL after being precipitated and redispersed several times whereas the aC QDs were very sensitive to the washing procedure, often losing their PL over time. The size increase observed from TEM cannot be used to make any conclusions about the presence of shells because the increase in diameter after shell growth is less than the uncertainty in the diameter. The small increase in the average diameter of the QDs after shell growth suggests that the ZnSe and ZnS shells are most likely incomplete. Histograms showing the size distribution for aC, aCS, and aCSS QD samples can be seen in Figures 1d–f, respectively.

4.2. Exciton Dynamics and Origin of Enhanced PL in aCSS. TRPL and TA spectroscopy measurements were carried out on all three samples to determine the effect of the shells on the exciton dynamics and gain insight into the origin of the significantly enhanced PL in the aCSS sample. In our previous work, CdSe QDs were compared to core/shell/shell CdSe/ZnSe/ZnS (CSS) QDs using TRPL, which showed that the CdSe QDs had an extra fast component of the PL decay due to nonradiative recombination that was eliminated in the CSS

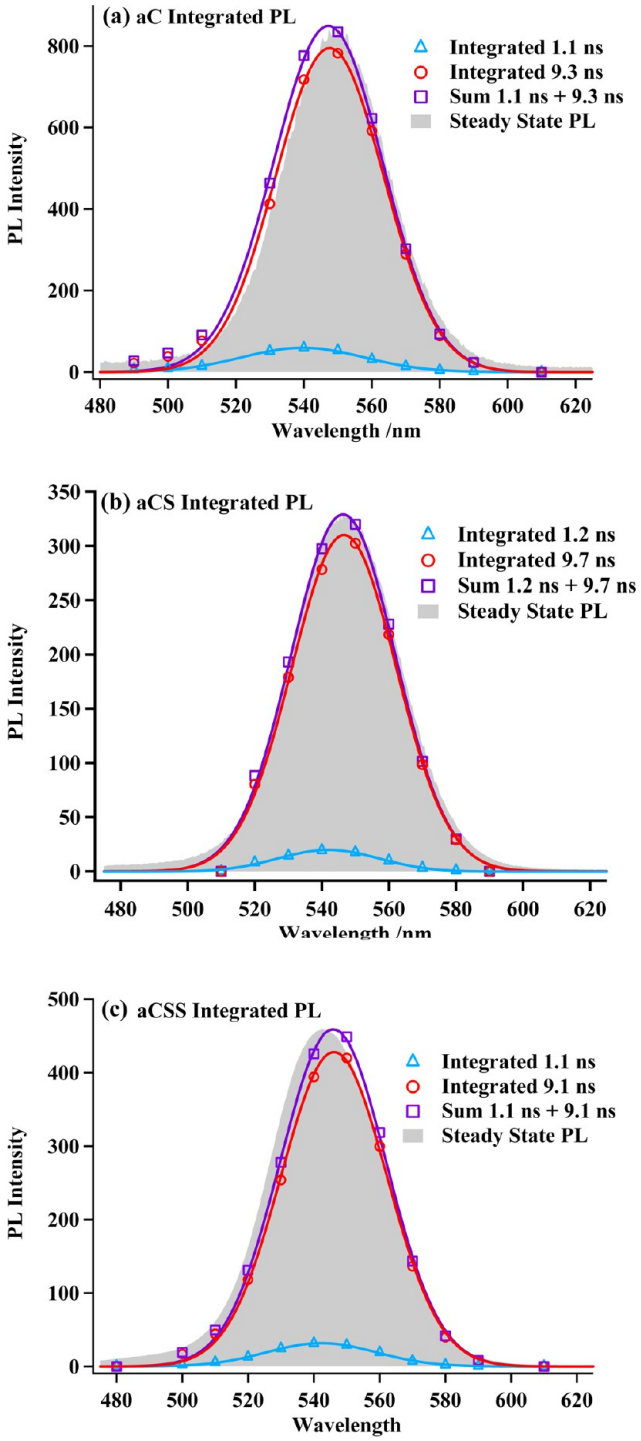

Figure 8. Global fitting results for the aC, aCS and aCSS QD TRPL data. The PL decay at each wavelength was separated into the two lifetime components and each one was integrated to get the photon flux from that component. The integrated PL from the two components are plotted vs wavelength and fit to Gaussian functions. The sum of the two Gaussians is compared to the normalized steady state PL spectrum.

sample.[19] Eliminating this recombination pathway was our explanation for the improved QY for the CSS sample. It was very surprising to see that in the cases of aC, aCS, and aCSS QDs, there was no significant difference in the TRPL between the three samples in spite of their significantly different quantum yields. All three samples show similar double exponential decays with lifetimes of about 1 and 9 ns. In all cases the majority of the PL is emitted via the slow (9 ns) component of the decay. The lower PL QY for the aC QDs relative to aCS and aCSS implies that there is higher probability for nonradiative recombination at the surface of aC and since an additional decay pathway was not observed in the TRPL, it likely occurs on a shorter time scale.

TA spectroscopy was used to probe the exciton dynamics on the ps time scale. We attribute the fastest (7 ps) component of the decay of the free electron and hole to bound electron−hole transition. Upon absorbing 480 nm light, electron−hole pairs are generated with energy well outside the band edges of the QDs and as the carriers cool and reach the bandedges they form bound electron−hole pairs, or excitons. The size dependent exciton binding energy of CdSe has been reported to be between 250 and 350 meV in our size range.[36] Taking the 7 ps B-spectrum dA minimum as the free electron spectrum and the medium length time constant dA minimum as the bound exciton, we calculate the exiton binding energy in the three systems to be 305 ± 10 meV. The medium lifetime component varies the most between samples: 55 ps for aC to 80 ps for aCS and aCSS. This component is attributed to nonradiative recombination through surface trap state or in the case of the aCS and aCSS, through lattice dislocations at the core/shell interface. The 700 ps and >2 ns (infinite) time constants used to describe the remaining TA signal is attributed to the excitons which recombine, mostly radiatively, on the nanosecond time scale. Carrier trapping is not observed in the TA signal as there is no dA absorption minimum shift in the B-spectrum from the medium to long to >2 ns decay features. From the single wavelength traces presented in Figure 6, it is clear that the TA signal for aC QDs has a much larger fast component amplitude than the aCS or aCSS samples. This observation is consistent with the aC samples having the lowest QY of the three samples studied, the majority of the aC recombination occurs nonradiatively.

Figure 9 contains a model showing the band positions of the three materials in the aCSS QDs. The curved valence and conduction band edges for the aC have been suggested previously[14,15] and provide a possible explanation for the unique optical properties of the aC, aCS, and aCSS samples. The alloying process employed to produce the aC QDs results in a gradient structure that is cadmium rich in the center and zinc rich near the surface. The cadmium-rich center, with its small bandgap, funnels excitons away from the surface of the QD. When an electron−hole pair is initially formed, the electron and hole have enough energy to access the surface of the nanocrystal and undergo trap-state mediated, nonradiative recombination. On the picoseconds time scale, the aC QDs have much faster exciton recombination than the aCS and aCSS QDs because the uncapped surface provides additional recombination pathways. The 540 nm TA decay traces in Figure 6 shows that after 1 ns the aC bleach has decayed to 1% of its original amplitude, whereas the aCS has 14%, and the aCSS 18% of the original bleach signal remaining. On the nanosecond time scale there is no significant difference in the dynamics because by that time all excitons have been funneled into the center of the aC where they no longer interact with surface traps.

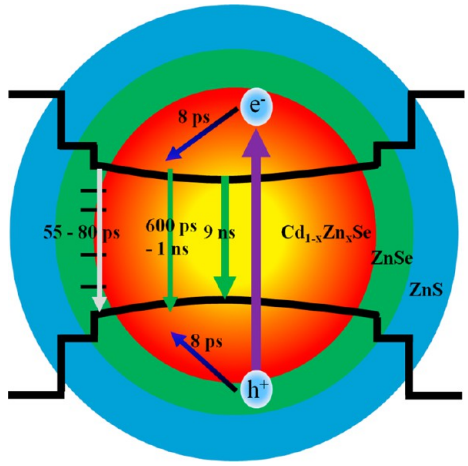

Figure 9. Schematic showing the band structure of an aCSS QD and lifetimes for various excitonic processes after absorption of a photon (purple arrow) with energy greater than the bandgap. The band edges are curved in the core to represent the gradient alloy structure where the center of the core is cadmium rich. Following absorption of a photon, carrier cooling occurs with an 8 ps lifetime. The exciton can then either undergo nonradiative recombination through surface related state (55−80 ps lifetime) or remain in the alloy core and recombine through either a 600 ps to 1 ns, nonradiative pathway or the 9 ns radiative process. Once excitons have relaxed to the bandedge in the core nanocrystal the graded alloy structure prevents excitons from reaching surface or interface traps. This diagram represents an ideal case of two complete shells of pure ZnSe and ZnS, in reality some of the QDs may have incomplete shells and the shells may also be an alloy of ZnSe and ZnS (ZnSeS).

5. CONCLUSIONS

We have demonstrated the synthesis of aCSS $Cd_{1-x}Zn_xSe$/ZnSe/ZnS QDs via a simple one pot approach. The resulting QDs are monodisperse, soluble in organic solvents and resistant to PL quenching during the washing procedure. PL measurements showed that the aC, aCS and aCSS QDs have similar PL spectra with a peak centered at 540 nm. The PL QY was 9.6% for aC, 42% for aCS, and 63% for aCSS, which is very high for QDs emitting green light. TA spectroscopy showed that nonradiative recombination occurs primarily on the 50 to 80 ps time scale and is more prevalent in the aC sample compared to the aCS and especially to the aCSS sample. The faster recombination rate is attributed to nonradiative recombination of free electron carriers at surface trap states that also decreases the PL QY. Interestingly, while the ps dynamics differ after adding shells to the aC QDs, the ns lifetime measured by TRPL is almost identical for the three samples. Herein, the surface trap state mediated nonradiative recombination observed in the alloyed QD sample was measured by TA spectroscopy to be in the 55 ps time scale and minimization of this component in the aCSS decay is correlated with enhanced PL QY.

■ AUTHOR INFORMATION

Corresponding Author

*E-mail: yhsu@cc.nctu.edu.tw (Y.-J.H.); zhang@ucsc.edu (J.S.Z.). Phone: +886 3 5712121 × 55317 (Y.-J.H.); (831) 459-3776 (J.S.Z.).

Author Contributions

†B.C.F. and Y.-C.P. contributed equally to this work.

Notes

The authors declare no competing financial interest.

■ ACKNOWLEDGMENTS

This work was supported by the BES Division of the US DOE (DE-FG02-05ER46232) and the National Science Council of Republic of China (Taiwan) under Grant NSC-101-2113-M-009-018, NSC-101-3113-P-009-005, and NSC-102-2917-I-009-042. Y.L. acknowledges the financial support by the NSF (United States) (DMR-0847786).

■ REFERENCES

(1) Peng, Z. A.; Peng, X. *J. Am. Chem. Soc.* **2002**, *124* (13), 3343–3353.
(2) Peng, Z. A.; Peng, X. *J. Am. Chem. Soc.* **2001**, *123* (1), 183–184.
(3) Caruge, J.; Halpert, J.; V Wood, V. B.; Bawendi, M. *Nat. Photonics* **2008**, *2* (4), 247–250.
(4) Sun, Q.; Wang, Y. A.; Li, L. S.; Wang, D.; Zhu, T.; Xu, J.; Yang, C.; Li, Y. *Nat. Photonics* **2007**, *1* (12), 717–722.
(5) Lopez-Luke, T.; Wolcott, A.; Xu, L.; Chen, S.; Wen, Z.; Li, J.; De La Rosa, E.; Zhang, J. Z. *J. Phys. Chem. C* **2008**, *112* (4), 1282–1292.
(6) Kamat, P. V. *J. Phys. Chem. C* **2008**, *112* (48), 18737–18753.
(7) Guijarro, N.; Lana-Villarreal, T.; Shen, Q.; Toyoda, T.; Gomez, R. *J. Phys. Chem. C* **2010**, *114* (50), 21928–21937.
(8) Medintz, I. L.; Uyeda, H. T.; Goldman, E. R.; Mattoussi, H. *Nat. Mater.* **2005**, *4* (6), 435–446.
(9) Medintz, I. L.; Berti, L.; Pons, T.; Grimes, A. F.; Douglas, S.; Alessandrini, A.; Facci, P.; Mattoussi, H. *Nano Lett.* **2007**, *7* (6), 1741–1748.
(10) Wang, X.; Ren, X.; Kahen, K.; Hahn, M. A.; Rajeswaran, M.; Maccagnano-Zacher, S.; Silcox, J.; Cragg, G. E.; Efros, A. L.; Krauss, T. D. *Nature* **2009**, *459* (7247), 686–9.
(11) David Battaglia, B. B.; Peng, X. *J. Am. Chem. Soc.* **2005**, *127*, 10889–10897.
(12) Blackman, B.; Battaglia, D.; Peng, X. *Chem. Mater.* **2008**, *20* (15), 4847–4853.
(13) Alivisatos, A. P. *J. Phys. Chem.* **1996**, *100* (31), 13226–13239.
(14) Regulacio, M. D.; Han, M. Y. *Acc. Chem. Res.* **2010**, *43* (5), 621–630.
(15) Ouyang, J.; Ratcliffe, C. I.; Kingston, D.; Wilkinson, B.; Kuijper, J.; Wu, X.; Ripmeester, J. A.; Yu, K. *J. Phys. Chem. C* **2008**, *112* (13), 4908–4919.
(16) Wang, X.; Ren, X.; Kahen, K.; Hahn, M. A.; Rajeswaran, M.; Maccagnano-Zacher, S.; Silcox, J.; Cragg, G. E.; Efros, A. L.; Krauss, T. D. *Nature* **2009**, *459* (7247), 686–689.
(17) Smith, A. M.; Nie, S. *Nat. Biotechnol.* **2009**, *27* (8), 732.
(18) Gul, S.; Cooper, J. K.; Corrado, C.; Vollbrecht, B.; Bridges, F.; Guo, J.; Zhang, J. Z. *J. Phys. Chem. C* **2011**, *115* (43), 20864–20875.
(19) Fitzmorris, R. C.; Cooper, J. K.; Edberg, J.; Gul, S.; Guo, J.; Zhang, J. Z. *J. Phys. Chem. C* **2012**.
(20) Mokari, T.; Banin, U. *Chem. Mater.* **2003**, *15* (20), 3955–3960.
(21) Hines, M. A.; Guyot-Sionnest, P. *J. Phys. Chem.* **1996**, *100* (2), 468–471.
(22) Lees, E. E.; Gunzburg, M. J.; Nguyen, T. L.; Howlett, G. J.; Rothacker, J.; Nice, E. C.; Clayton, A. H. A.; Mulvaney, P. *Nano Lett.* **2008**, *8* (9), 2883–2890.
(23) Reiss, P.; Bleuse, J.; Pron, A. *Nano Lett.* **2002**, *2* (7), 781–784.
(24) Peng, X.; Schlamp, M. C.; Kadavanich, A. V.; Alivisatos, A. *J. Am. Chem. Soc.* **1997**, *119* (30), 7019–7029.
(25) Dabbousi, B. O.; Rodriguez-Viejo, J.; Mikulec, F. V.; Heine, J. R.; Mattoussi, H.; Ober, R.; Jensen, K. F.; Bawendi, M. G. *J. Phys. Chem. B* **1997**, *101* (46), 9463–9475.
(26) Jones, M.; Lo, S. S.; Scholes, G. D. *Proc. Natl. Acad. Sci. U.S.A.* **2009**, *106* (9), 3011.
(27) Reiss, P.; Carayon, S.; Bleuse, J.; Pron, A. *Synth. Met.* **2003**, *139* (3), 649–652.
(28) Sun, Y. H.; Liu, Y. S.; Vernier, P. T.; Liang, C. H.; Chong, S. Y.; Marcu, L.; Gundersen, M. A. *Nanotechnology* **2006**, *17*, 4469.
(29) Talapin, D. V.; Mekis, I.; Goetzinger, S.; Kornowski, A.; Benson, O.; Weller, H. *J. Phys. Chem. B* **2004**, *108* (49), 18826–18831.
(30) Lee, H.; Yang, H.; Holloway, P. H. *J. Lumin.* **2007**, *126* (2), 314–318.
(31) Kemsley, J.; Washington, C. *Chem. Eng. News* **2009**, *87*, 29–31.
(32) Magde, D.; Wong, R.; Seybold, P. G. *Photochem. Photobiol.* **2002**, *75* (4), 327–334.
(33) Newhouse, R. J.; Wang, H.; Hensel, J. K.; Wheeler, D. A.; Zou, S.; Zhang, J. Z. *J. Phys. Chem. Lett.* **2011**, *2*, 228–235.
(34) Corrado, C.; Cooper, J. K.; Zhang, J. Z. *Sci. Adv. Mater.* **2012**, *4* (2), 254–265.
(35) Yu, W. W.; Qu, L.; Guo, W.; Peng, X. *Chem. Mater.* **2003**, *15* (14), 2854–2860.
(36) Meulenberg, R. W.; Lee, J. R. I.; Wolcott, A.; Zhang, J. Z.; Terminello, L. J.; van Buuren, T. *ACS Nano* **2009**, *3* (2), 325–330.